Structural basis of Rad53 kinase activation by dimerization and activation segment exchange

ARTICLE *in* CELLULAR SIGNALLING · MAY 2014

Impact Factor: 4.32 · DOI: 10.1016/j.cellsig.2014.05.004 · Source: PubMed

7 AUTHORS, INCLUDING:

Derek F J Ceccarelli

Samuel Lunenfeld Research Institute

34 PUBLICATIONS **1,344** CITATIONS

SEE PROFILE

Jane Mcglade

SickKids

101 PUBLICATIONS **9,950** CITATIONS

SEE PROFILE

Cellular Signalling 26 (2014) 1825–1836

Contents lists available at ScienceDirect

Cellular Signalling

journal homepage: www.elsevier.com/locate/cellsig

Structural basis of Rad53 kinase activation by dimerization and activation segment exchange ☆

Leanne E. Wybenga-Groot [a,*,1], Cynthia S. Ho [b,1], Frédéric D. Sweeney [b,c], Derek F. Ceccarelli [b], C. Jane McGlade [a], Daniel Durocher [b,c,**], Frank Sicheri [b,c,***]

[a] The Arthur and Sonia Labatt Brain Tumour Research Centre and Program in Cell Biology, The Hospital for Sick Children, 555 University Avenue, Toronto, ON M5G 1X8, Canada
[b] The Lunenfeld-Tanenbaum Research Institute, Mount Sinai Hospital, 600 University Avenue, Toronto, Ontario M5G 1X5, Canada
[c] Molecular Genetics, University of Toronto, Toronto, Ontario M5S 1A8, Canada

ARTICLE INFO

Article history:
Received 22 April 2014
Accepted 2 May 2014
Available online 9 May 2014

Keywords:
Chk2
Checkpoint kinase 2
CHEK2

ABSTRACT

The protein kinase Rad53 is a key regulator of the DNA damage checkpoint in budding yeast. Its human ortholog, CHEK2, is mutated in familial breast cancer and mediates apoptosis in response to genotoxic stress. Autophosphorylation of Rad53 at residue Thr354 located in the kinase activation segment is essential for Rad53 activation. In this study, we assessed the requirement of kinase domain dimerization and the exchange of its activation segment during the Rad53 activation process. We solved the crystal structure of Rad53 in its dimeric form and found that disruption of the observed head-to-tail, face-to-face dimer structure decreased Rad53 autophosphorylation on Thr354 *in vitro* and impaired Rad53 function *in vivo*. Moreover, we provide critical functional evidence that Rad53 trans-autophosphorylation may involve the interkinase domain exchange of helix αEF *via* an invariant salt bridge. These findings suggest a mechanism of autophosphorylation that may be broadly applicable to other protein kinases.

1. Introduction

The safeguarding of genomic integrity is an essential process whose failure can lead to cell death, gross chromosomal rearrangements or mutations [1]. In vertebrates, genomic stability requires the detection, signaling and repair of DNA damage, and a failure to do so is strongly associated with tumorigenesis [1]. When cells are exposed to DNA damage and in particular to DNA double-strand breaks (DSBs), cells mount an evolutionarily conserved response that coordinates DNA repair and initiates a slow down or arrest of the cell cycle, an event termed the DNA damage checkpoint.

In eukaryotes, the DNA damage checkpoint is initiated when kinases of the ATM/ATR family are activated by DNA lesion sensors [2]. Genetic studies in budding yeast have identified the serine/threonine protein kinase Rad53 and its mammalian ortholog checkpoint kinase 2 (Chk2, product of gene *CHEK2*) as key regulators of the DNA damage checkpoint [3,4]. Loss-of-function mutations of *RAD53* result in loss of viability due to an essential function in maintaining dNTP levels during DNA replication, but hypomorphic *RAD53* mutations result in DNA damage sensitivity and deficits in nearly all checkpoint responses in yeast [5–9]. Similarly, loss-of-function mutations in the mammalian tumor suppressor *CHEK2* also lead to a defective checkpoint response as well as deficiencies in DNA damage-induced apoptosis [10–12].

Rad53 belongs to a subfamily of protein kinases characterized by the presence of one or more phospho-threonine recognition modules known as forkhead-associated (FHA) domains [6,13–15] (Fig. 1A). Rad53 contains two FHA domains, FHA1 and FHA2, which flank a central serine/threonine protein kinase domain [15]. Also, Rad53 contains two serine–glutamine/threonine–glutamine cluster domains (SCD) located N-terminal to FHA1 and immediately C-terminal to the kinase [10,16]. Mammalian Chk2 is similarly organized but notably with only one SCD and one FHA domain N-terminal to the kinase domain [10,11]. Within the SCD of Rad53 and Chk2 are clusters of serine–glutamine and threonine–glutamine (SQ/TQ) motifs. The SQ/TQ motifs are potential target phosphorylation sites of the PI(3) kinase-like protein kinase

Abbreviations: AMPPNP, adenylylimidodiphosphate; AUC, analytical ultracentrifugation; βME, β-mercaptoethanol; Chk2, checkpoint kinase 2; DAPK3, Death-associated protein kinase 3; DTT, dithiothreitol; FHA, forkhead-associated; HU, hydroxyurea; IPTG, Isopropyl β-D-1-thiogalactopyranoside; LOK, lymphocyte-originated kinase; MAPK, mitogen-activated protein kinase; OSR1, oxidative stress-responsive-1; SLK, STE20-like kinase; TEV, tobacco etch virus.

☆ The authors declare no conflict of interest.

* Corresponding author. Tel.: +1 416 813 8658.
** Corresponding author. Tel.: +1 416 586 4800x2544.
*** Correspondence to: F. Sicheri, The Lunenfeld-Tanenbaum Research Institute, Mount Sinai Hospital, 600 University Avenue, Toronto, Ontario M5G 1X5, Canada. Tel.: +1 416 586 8471.
E-mail addresses: leanne.wybenga.groot@utoronto.ca (L.E. Wybenga-Groot), cynthia.sw.ho@gmail.com (C.S. Ho), frederic.sweeney@gmail.com (F.D. Sweeney), ceccarelli@lunenfeld.ca (D.F. Ceccarelli), jmcglade@sickkids.ca (C.J. McGlade), durocher@lunenfeld.ca (D. Durocher), sicheri@lunenfeld.ca (F. Sicheri).

[1] Authors contributed equally to this work.

http://dx.doi.org/10.1016/j.cellsig.2014.05.004
0898-6568/

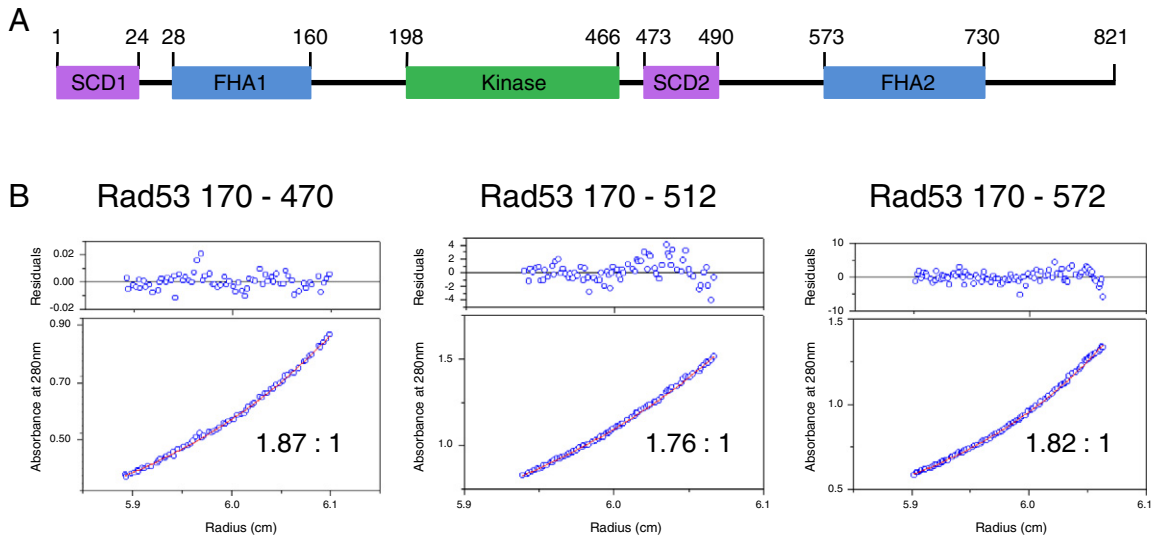

Fig. 1. The Rad53 kinase domain is sufficient for dimerization. (A) The domain structure of Rad53. (B) Data from analytical ultracentrifugation sedimentation equilibrium experiments are shown for Rad53 proteins. The data points depicted were collected at 10,000 rpm and 20 °C for 170–470, 4 °C for 170–512 and 170–572. The red lines in the lower panels correspond to the fit of the data to a monodisperse dimeric model. The residual deviations from the theoretical fits are given in the upper panels.

family members Mec1 and Tel1 in yeast, fungal orthologs of mammalian ATR and ATM respectively, which act upstream of Rad53 and Chk2 as DNA damage sensor proteins [2,17].

Activation of Rad53 *in vivo* requires its phospho-dependent interaction with the signaling adaptors Rad9 and Mrc1 [15,18,19]. The Rad53–Rad9 interaction is FHA-dependent and occurs following Mec1-dependent phosphorylation of Rad9 at multiple threonine residues [19–21]. Rad9 bound Rad53 proteins are phosphorylated at multiple sites (within the SCD1 by Mec1), which primes Rad53 for activation. Rad53 subsequently undergoes extensive autophosphorylation that is likely facilitated by the clustering of multiple Rad53 molecules on hyperphosphorylated Rad9 [22]. In particular, autophosphorylation of a key regulatory site in the activation segment, Thr354, is required for the catalytic activation of Rad53.

Similar to Rad53, activation of Chk2 kinase requires phosphorylation of a key threonine (Thr383) in the activation segment [23,24]. Notably, dimerization is also necessary for Chk2 activation, possibly by promoting efficient trans-autophosphorylation of the activation segment. Upon DNA damage, Thr68 within the SCD is phosphorylated, which promotes oligomerization of Chk2 *via* the FHA domain and leads to phosphorylation on Thr383 and Thr387 [23–28]. A crystal structure of Chk2 consisting of the FHA and kinase domains revealed a dimer conformation involving intermolecular FHA–kinase and FHA–FHA interactions. In the dimer, the kinase active sites are face-to-face in close proximity and in an arrangement that would facilitate trans-autophosphorylation of their activation loops [29]. A crystal structure of the isolated Chk2 kinase domain revealed a different dimer configuration, in which the kinase domains are positioned tail-to-tail and the activation segments are exchanged between protomers [30]. Intermolecular strand exchange has been observed in the dimeric crystal structures of other protein kinases, including p38α MAP kinase, p70 ribosomal S6 kinase (p70S6K), death-associated protein kinase 3 (DAPK3) and three sterile kinase (STE) family members, namely STE20-like kinase (SLK), lymphocyte-originated kinase (LOK), and oxidative stress-responsive-1 (OSR1) kinase [31–35]. While it has been proposed that activation segment exchange may be a common mechanism for dimerization-driven activation by trans-autophosphorylation, further experimental work is required to fully validate this mechanism of regulation [30,32].

The objective of this study was to understand the mechanisms leading to Rad53 activation by assessing the contribution of dimerization and activation segment exchange in this process. We first found that Rad53 dimerizes in solution and then solved the crystal structure of the Rad53 kinase domain in its dimeric form. The crystal structure reveals a head-to-tail, face-to-face mode of dimerization that is necessary for autophosphorylation of Thr354 on the Rad53 activation loop, as confirmed by *in vitro* and *in vivo* functional analyses. Also, our results provide evidence that Rad53 trans-autophosphorylation may involve the intermolecular exchange of helix αEF *via* an invariant salt bridge, indicating a mechanism of autophosphorylation that may be broadly applicable to other protein kinases.

2. Materials and methods

2.1. Cloning, strains, expression and purification

Overexpression of wild-type (WT) Rad53 from *Saccharomyces cerevisiae* is toxic to bacteria. We serendipitously identified an attenuating mutant Ala225 to serine (A225S) that expressed well in bacteria while remaining catalytically competent for Thr354 autophosphorylation and phosphorylation of a generic myelin basic protein substrate *in vitro*. The A225S form of Rad53 was used as our WT reference and as a template for the generation of mutants for *in vitro* biochemical analyses. *In vivo* studies employed true WT Rad53 as a reference and for the generation of mutants tested *in vivo*. Rad53 constructs were generated by PCR into pPROEx-Hta-TEV and mutants by QuikChange site-directed mutagenesis (Stratagene).

Rad53 constructs were individually transformed into *Escherichia coli* BL-21 cells and grown in LB media supplemented with 100 μg/ml ampicillin overnight at 15 °C (A_{600} = 0.6, 0.2 mM IPTG induction). Cells were collected by centrifugation, resuspended in buffer A (20 mM HEPES pH 7.5, 200 mM NaCl, 5 mM imidazole) supplemented with 1 mg/ml lysozyme and 5 mM βME, and lysed by sonication on ice. Following centrifugation and filtering to remove cell debris, crude lysate was applied to a HiTrap chelating HP Ni column (Pharmacia). Non-specifically bound proteins were removed by consecutive washes using five column volumes of 5 mM and 30 mM imidazole buffer (20 mM HEPES pH 7.5, 200 mM NaCl) and the 6×HIS-Rad53 proteins eluted with 350 mM imidazole buffer. Removal of the 6×HIS-tag was achieved by addition of 6×HIS-TEV (tobacco etch virus) protease (non-cleavable HIS-tag), 1 mM DTT and 0.5 mM EDTA directly to the final 350 mM imidazole wash fraction (overnight, 4 °C). Following dialysis to remove DTT and imidazole, the TEV-cleaved sample was applied to a Ni column and the Rad53 protein in the flow-through concentrated by ultrafiltration and further purified by gel filtration chromatography (20 mM HEPES

pH 7.5, 100 mM NaCl, 2 mM DTT). Aliquots were flash frozen in liquid nitrogen and stored at −80 °C until required. Yeast strains were derived from W303a as described elsewhere [36]. Additional strains were generated by standard yeast genetic techniques.

2.2. Analytical ultracentrifugation

Rad53 with A225S and an inactivating mutation (D339A) was used as WT reference. The sedimentation equilibrium of Rad53 proteins was run at 4 °C or 20 °C, typically at speeds of 10,000, 12,000 and 15,000 rpm, at the University of Toronto, Department of Biochemistry core facility. Data collected at 10,000 and 15,000 rpm were analyzed for the highest and middle concentration samples. The plots of ln(abs) *versus* the radius square were analyzed to assess if the sample was composed of mainly one species. Global self-association was analyzed using Origin software (Beckman) to determine the average observed molecular weight of the protein. Also determined was the ratio of the observed molecular weight to the calculated molecular weight based on protein sequence and a best-fit two state equilibrium model.

2.3. Crystallization, data collection, structure determination and modeling

A Rad53 construct containing the kinase domain with an inactivating mutation and SCD2 (residues 170–512, D339A/A225S; $Rad53^{170–512:Dead}$, herein referred to as Rad53) crystallized at 20 °C by the hanging drop diffusion method by mixing 0.5 μl of protein (30 mg/ml) with 0.5 μl of well solution (30% v/v PEG_{400}, 50 mM sodium citrate, 100 mM Tris pH 8.0). Crystals of Rad53 with the non-hydrolysable ATP analog adenylylimidodiphosphate (AMPPNP) were obtained by co-crystallization in the presence of 5 mM AMPPNP and 20 mM $MgCl_2$. Crystals were stabilized by glutaraldehyde crossing–linking treatment for 10 min [37] prior to flash freezing in liquid nitrogen. Diffraction data for the apo crystal was collected at the National Synchrotron Light Source (Brookhaven National Laboratory, Long Island, NY) beamline X29 using an ADSC Q315 detector; diffraction data for the AMPPNP crystal was collected at the Advanced Photon Source (Argonne National Laboratory, Argonne, IL) on the BioCARS 14ID-B beamline using an ADSC Q315 detector. Data processing and reduction were carried out with the HKL and XDS program suites [38,39]. The Rad53 structure was solved by molecular replacement with CNS using the human DAPK structure (PDB: 1IG1) as a search model, followed by iterative cycles of model building with O and Coot and structure refinement with CNS, REFMAC5, and Phenix [40–44].

2.4. Generation of phosphospecific $Rad53^{pT354}$ antibody

A polyclonal rabbit antibody specific to phosphorylated Ser350 and Thr354 (α-$Rad53^{pT354}$) of Rad53 was generated by injecting three animals with a cationic BSA-coupled phosphopeptide corresponding to the Rad53 phosphorylated activation segment (sequence G–N–G–pS–F–M–K–pT–F–C–G). The specificity of the various sera was tested by standard ELISA techniques using serum from a rabbit injected with unphosphorylated peptide as a benchmark control. Phosphospecific anti-sera were purified using an agarose column containing KLH-coupled phosphorylated peptides. Coupling was performed using the Imject Maleimide-Activated Bovine Serum Albumin Kit (Pierce Biotechnology, #77116) and the agarose column and purification methods were performed using SulfoLink Immobilization (Pierce Biotechnology Kit #44995) as per the manufacturer's instructions.

2.5. In vitro kinase assay and immunoblotting

Purified Rad53 protein was diluted in kinase reaction buffer (50 mM HEPES pH 7.5, 250 mM NaCl, 20 mM $MgCl_2$, 20 mM $MnCl_2$, 2 mM DTT) and incubated with purified 6×HIS-tag full-length kinase inactive (D339A) Rad53 in the presence of 1 mM ATP at room temperature. Reactions were stopped at various time points by mixing and boiling with SDS loading buffer, resolved by SDS-PAGE, and transferred to PVDF membrane. The membrane was blocked with 5% milk in TBS-T (0.1%; 1 h) and trans-autophosphorylation of Thr354 detected by immunoblotting with α-$Rad53^{pT354}$ (1:1000; 45 min) followed by incubation with HRP-conjugated goat α-rabbit (1:10,000; 30 min) and visualization by chemiluminescence (Super Signal West Pico, Pierce). Total Rad53 protein levels were detected by immunoblotting with the polyclonal Rad53 antibody DAB001 [45].

2.6. DNA damage sensitivity assays

Hydroxyurea (HU) was purchased from Sigma-Aldrich Chemicals. Spot tests were performed using five-fold serial dilutions of an overnight yeast culture. An 8 μl aliquot of the diluted culture was spotted on corresponding dropout media plates with or without genotoxins (see figure legends for details) and was grown for 3–4 days at 30 °C.

3. Results

3.1. Rad53 exists as a dimer in solution

To investigate the role of dimerization in the regulation of Rad53 kinase activity, we purified multiple deletion constructs of Rad53 protein for biochemical and biophysical analyses. During purification, the Rad53 proteins eluted on gel filtration chromatography larger than expected for a monomer. To investigate the precise oligomerization status of Rad53 in solution we performed sedimentation equilibrium analyses. We found that Rad53 protein consisting of the kinase domain (residues 170–470), the kinase domain plus SCD2 (residues 170–512), or the kinase domain, SCD2, and the SCD2-FHA2 linker (residues 170–572) existed as dimers in solution as evidenced by a near 2:1 ratio of the experimentally observed molecular weight *versus* the calculated monomer molecular weight (Fig. 1 and Table 1). This indicated that the Rad53 kinase domain can form dimers in solution, and that the kinase domain is sufficient for dimerization.

3.2. Description of Rad53 crystal structure

To investigate the molecular basis of Rad53 dimerization, we set out to crystallize Rad53 kinase. A construct encompassing residues 170–512 and a kinase-inactivating mutation (D339A/S225A; $Rad53^{170–512:Dead}$, herein referred to as Rad53) yielded crystals both in the apo form and in complex with AMPPNP. Diffraction data were collected to 2.7 Å and 2.9 Å, respectively, and the structures were solved by molecular replacement using human DAPK (PDB: 1IG1) as a search model. A structure-based protein sequence alignment of Rad53 orthologs and human homologs is shown in Fig. 2. Both the apo and nucleotide-bound structures of Rad53 contain two Rad53 molecules in the asymmetric unit and are very similar in conformation, (root mean square deviations (rmsd) of

Table 1
Analytical ultracentrifugation analyses of Rad53 proteins.

Rad53	Residues	MWobs[a]	MWcalc[b]	Ratio[c]	Model[d]
WT[e]	170–470	62.8	33.6	1.87:1	Dimer
WT	170–512	67.2	38.3	1.76:1	Dimer
WT	170–572	81.9	45.1	1.82:1	Dimer
WT	170–512	75.0	38.3	1.95:1	Dimer
DDD / AAA	170–512	76.9	38.2	2.01:1	Dimer
AAQ	170–512	79.7	38.2	2.08:1	Dimer
AAQ + DDD / AAA	170–512	37.3	38.0	0.98:1	Monomer

[a] Observed global self-association of the sample as an average molecular weight in kDa.
[b] Calculated theoretical molecular weight of the monomer based on protein sequence in kDa.
[c] Ratio of observed molecular weight to monomeric molecular weight.
[d] Best-fit equilibrium model.
[e] The D339A/A225S form of Rad53 was used as WT reference.

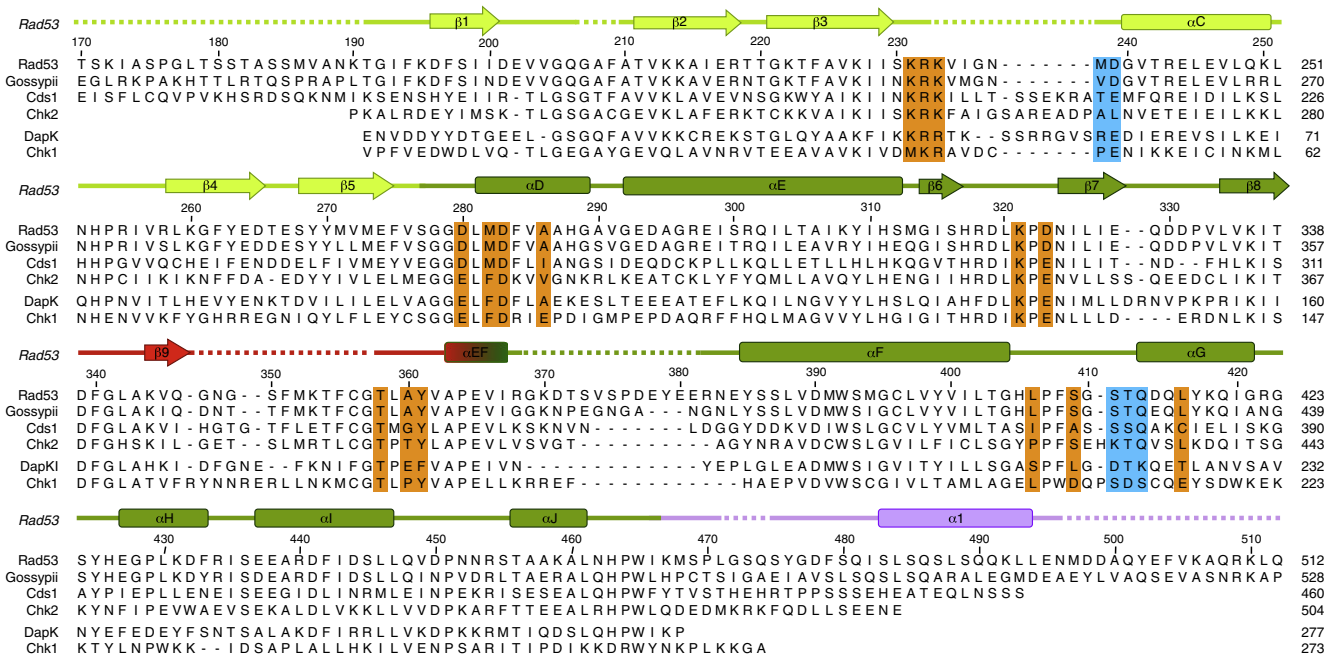

Fig. 2. Structure-based sequence alignment of Rad53 with yeast (*Ashbya gossypii* GI: 74695031 and *Schizosaccharomyces pombe* Cds1 GI: 2689196) and human (Chk2, DapK, and Chk1) orthologs, with residue numbering based on Rad53. The secondary structure elements of Rad53 are indicated, with the N-lobe, C-lobe, activation segment, and SCD2 colored light green, dark green, red and purple, respectively. Residues highlighted with orange or turquoise are involved in the KRK/DDD or STQ interface, respectively.

0.54 Å and 0.60 Å for molecules A and B main chain atoms, respectively), with the exception that electron density for the AMPPNP molecule can be seen in the ATP-binding pocket of the latter (Fig. 3A). Herein, Rad53 descriptions are based on the higher resolution apo-Rad53 structure. Data collection and refinement statistics for Rad53 structures are listed in Table 2.

Rad53 displays the typical bilobal architecture of other protein kinase domains (Fig. 3B). The smaller N-terminal lobe (N-lobe) consists of a twisted β-sheet and helix αC whereas the larger C-terminal lobe (C-lobe) consists of a series of eight α-helices (αD to αJ) capped by a two-strand (β7–β8) β-sheet. The majority of the SCD2 region is well ordered, consisting of a connector sequence (residues 475–482) and helix α1 (residues 483–494) that associate with the backside of the kinase C-lobe away from the active site (Fig. 3B). No discernable electron density was observed for a number of loop regions, including the N-terminal 21 residues preceding the kinase domain (170 to 190), residues 207 to 209 of the glycine-rich loop β1–β2 in molecule B (201 to 209 in molecule A), residues 234 to 237 of loop β3–αC (232 to 238 in molecule B), residues 347 to 357 of the activation segment, residues 369 to 381 of loop αEF–αF, residues 472 to 474, and the C-terminal 16 residues (497 to 512). Notably, due to disorder of the loops connecting helix αEF to the kinase domain, we cannot unequivocally determine whether helix αEF lies in an intramolecular position, as shown in Fig. 3A, or is intermolecularly exchanged with a neighboring Rad53 molecule in the crystal environment.

Rad53 adopts a canonical closed conformation of the kinase domain, with a conserved salt bridge between Lys227 (subdomain II) of strand β3 and Glu244 (subdomain III) of helix αC (Fig. 3B) [46]. Other conserved elements including the DFG motif (residues 339 to 341, with D339A), the APE motif (residues 363 to 365), and the catalytic base (Asp319) are well positioned for phosphoryl transfer function. Furthermore, the N-terminal portion of the activation segment adopts a configuration very similar to the canonical active state, with strand β9 (residues 344 to 346) forming a β-sheet with strand β6 (residues 314–316). However, the central portion of the activation loop including Thr354 is disordered, as well as the arginine side chain (Arg318) from the conserved HRD motif and residues of the glycine-rich loop β1–β2, both of which are important in stabilizing the nucleotide phosphate groups for phosphoryl transfer.

3.3. Rad53 dimerizes in a face-to-face configuration

Consistent with Rad53 existing as dimers in solution, Rad53 adopts a two-fold symmetric, antiparallel face-to-face (N-lobe to C-lobe) dimer configuration in the crystal lattice (Fig. 3C). The Rad53 asymmetric unit contains two molecules, A and B, whose overall folds are very similar (rmsd 0.38 Å main chain atoms). Application of crystal symmetry to molecules A and B generates two face-to-face dimers (1: A/A′ and 2: B/B′) with loop β3–αC of one kinase N-lobe packing against C-lobe elements of an opposing kinase protomer. Although the disordered nature of several residues and/or sidechains within the interkinase region prevents identification of specific interactions, two potential interfaces are predicted to be important based on proximity and conservation amongst Rad53 orthologs (Fig. 2). At the first interface, residues Met238 and Asp239 in the N-lobe of the first protomer pack against Ser411/Thr412/Gln413 (STQ) in the C-lobe of the second protomer (Fig. 3C). At the second interface, residues Lys231, Arg232, and Lys233 (KRK) of the N-lobe of the first protomer are proximal to a C-lobe pocket formed by residues from helix αD, loop β6–β7, the activation segment, loop αF–αG, and helix αG (Fig. 3C). In particular, this interface is characterized by charge complementarity of basic residues KRK of the first protomer and conserved acidic residues Asp280, Asp283, and Asp323 (DDD) of the second protomer. Notably, these STQ, KRK, and DDD elements are well conserved amongst Rad53 orthologs (Fig. 2).

Rad53 dimerization may involve molecular exchange of helix αEF between Rad53 protomers. As mentioned above, due to disorder of the loops connecting helix αEF to the kinase domain, we cannot ascertain if helix αEF lies in an intramolecular position or is intermolecularly exchanged with a neighboring Rad53 molecule. The distance between the carboxyl group of Gln346 and the amino group of Thr358 is ~28.4 Å, a distance that could readily be spanned by the eleven intervening disordered residues. Likewise, the ~26.0 Å between the carboxyl

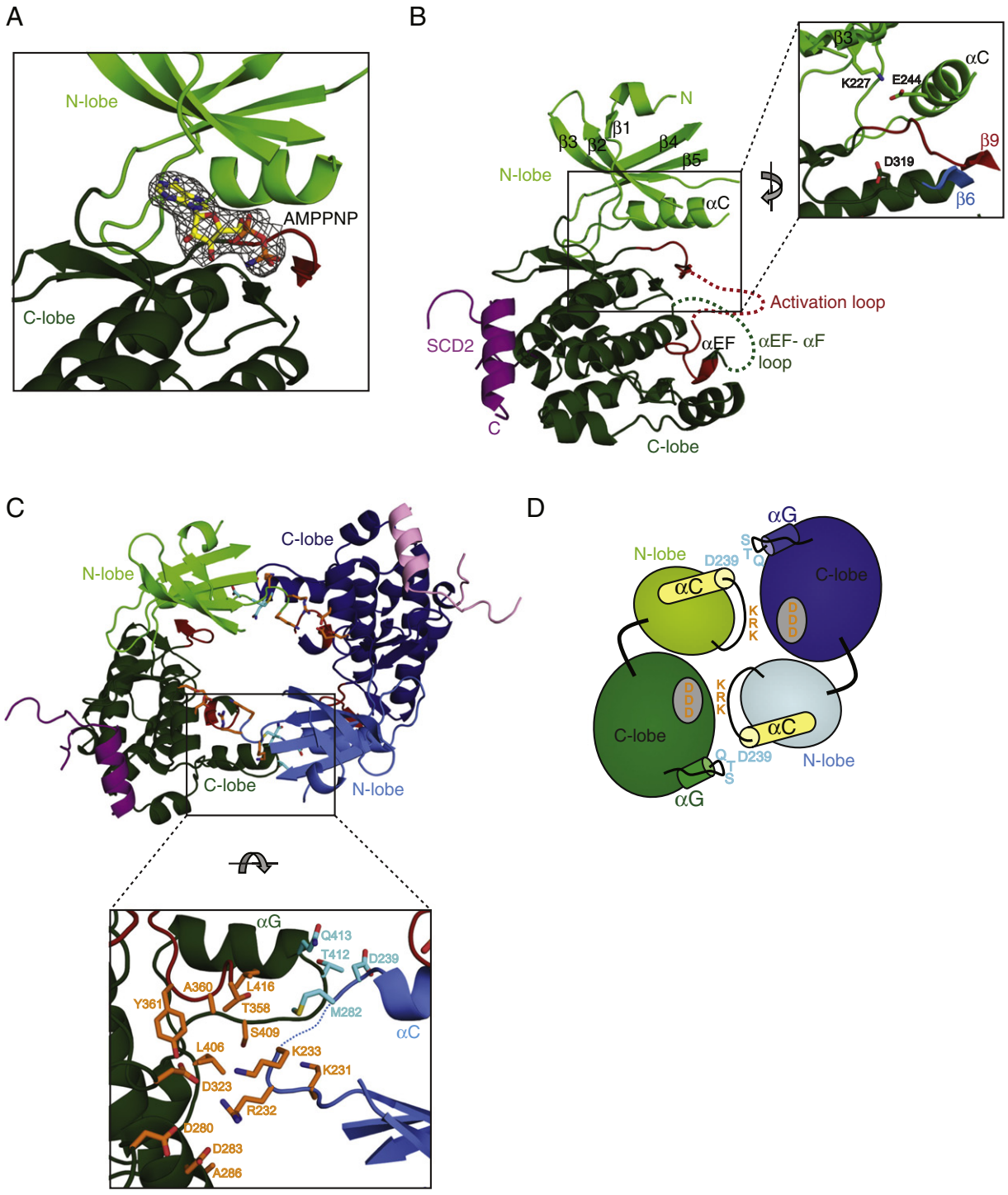

Fig. 3. Crystal structure of Rad53 kinase domain. (A) Ribbon representation of the Cα atoms of the Rad53 kinase domain bound to AMPPNP, with the electron density surrounding the AMPPNP molecule shown. (B) Ribbon representation of the Cα atoms of the Rad53 kinase domain and SCD2, with the N-lobe, C-lobe, activation segment, and SCD2 colored as in Fig. 2. Disordered loops connecting helix αEF to the kinase domain are represented by hatched lines. The boxed area is magnified, with key residues shown in stick. Carbon atoms are colored according to their respective origins; oxygen and nitrogen atoms are colored red and blue, respectively. Strands β6 and β9 are colored light blue and red, respectively. (C) Ribbon representation of the Cα atoms of the Rad53 kinase dimer, with the first protomer colored as in B. The N-lobe, C-lobe, activation segment, and SCD2 of the second protomer are colored light blue, dark blue, red and pink, respectively. The boxed area is magnified, with residues proximal to the dimer interface modeled and shown as stick. Carbon atoms involved in the KRK/DDD or STQ interface are colored orange or turquoise, respectively, as in Fig. 2. Oxygen and nitrogen atoms are colored red and blue, respectively. A hatched line represents disordered residues of loop β3αC. (D) Cartoon representation of the dimer interfaces, colored as in C. All ribbon diagrams were prepared with Pymol (The PyMOL Molecular Graphics System, Version 1.5.0.4 Schrödinger, LLC).

group of Ile367 and the amino group of Asn383 could readily be spanned by the fifteen intervening disordered residues.

While the overall configurations of Rad53 dimers 1 and 2 are very similar (rmsd 0.77 Å), superposition of molecule B of each dimer reveals minor differences in the position of molecule A with respect to molecule B (Fig. 4A). Residues at the face-to-face kinase interface exhibit positional shifts in the range of 1.5–2.2 Å. This plasticity suggests that the Rad53 dimer interface is inherently flexible or transient in nature.

Table 2
Data collection and refinement statistics.

	Rad53 Apo	Rad53 AMPPNP
Data collection		
PDB accession code	4PDP	4PDS
Space group	$C222_1$	$C222_1$
Cell dimensions		
a, *b*, *c* (Å)	76.43, 79.07, 227.71	74.15, 77.54, 222.17
α, β, γ (°)	90, 90, 90	90, 90, 90
Resolution (Å)	2.6	2.9
R_{merge}	6.7 (51.6)[a]	9.7 (64.8)
I / σI	15.3 (2.4)	21.6 (2.8)
Completeness (%)	94.5 (70.2)	98.7 (97.8)
Redundancy	6.1 (3.0)	8.5 (7.5)
Refinement		
Resolution (Å)	29.9–2.6	29.2–2.9
No. reflections	21,720	14,317
R_{work} / R_{free}	22.7/26.1	22.7/26.3
No. atoms		
Protein	3880	3564
Ligand	0	50
B-factors (Å^2)	101.6	90.7
R.m.s deviations		
Bond lengths (Å)	0.003	0.005
Bond angles (°)	0.613	0.894
Ramachandran		
Favored (%)	96.4	93.2
Allowed (%)	99.2	99.0

[a] Highest resolution shell is shown in parenthesis.

3.4. Rad53 dimerizes in a manner similar to human Chk2

Two crystal structures of the human Chk2 kinase domain were previously determined, revealing two different modes of face-to-face dimerization. While the structure of the isolated Chk2 kinase domain displayed a parallel or tail-to-tail crystallographic dimer, the structure of Chk2 consisting of the FHA and kinase domains revealed an antiparallel mode of dimerization similar to that observed for the Rad53 kinase domain [29,30].

The structure of human Chk2 consisting of the FHA and kinase domains has been solved in two different crystal forms, the first containing one dimer (PDB: 3I6U) and the second containing four dimers (PDB: 3I6W). Both crystal forms revealed an intertwined, domain-exchanged dimer involving intermolecular FHA–kinase and FHA–FHA interactions [29]. Superposition of the Rad53 and Chk2 (PDB: 3I6W or 3I6U) kinase domains confirms similar overall folds, although Chk2 adopts a slightly more open conformation with helix αC laterally displaced from the catalytic cleft (Fig. 4B) [29]. Notably, the N-terminal portion of the activation segment adopts the same "active" configuration [47] in Rad53 and Chk2 molecule B of PDB 3I6W (the activation segment adopts an alternate conformation in Chk2 molecule A of PDB 3I6W and in PDB 3I6U), and residues 388 to 397 including helix αEF of the Chk2 activation segment superimpose with residues 358 to 367 of the Rad53 activation segment in both Chk2 dimers (Fig. 4B). Similar to Rad53, Chk2 exhibits disorder in the loops connecting helix αEF to the kinase domain, supporting the possibility of intermolecular strand exchange in Chk2 [29].

Comparison of the Rad53 kinase dimer and the Chk2 FHA/kinase dimer revealed that the kinase domains dimerize in a similar head-to-tail, face-to-face manner, with the N-lobe of the first kinase protomer packed against elements of the C-lobe of the second kinase protomer (Fig. 4C). Consistent with our findings for Rad53, when molecule B of each dimer is superimposed, the conserved N-lobe KRK motif of the first Chk2 kinase protomer packs against a pocket on the C-lobe of the second protomer (Fig. 4D) [29]. Similar to Rad53, this pocket contains the conserved acidic DDD element (EDE in Chk2) formed by residues from helix αD and loop β6–β7, and residues from the activation segment and loop αF–αG (Fig. 4D). Also, the STQ motif of loop αF–αG of the first Chk2 protomer is positioned proximal to loop β3–αC of the second Chk2 protomer, although this interface is disturbed to some degree by the displacement of helix αC in Chk2 (Fig. 4D).

The finding of similar face-to-face modes of dimerization across human and yeast orthologs suggests that the mode of dimerization may be functionally relevant. Similar to our observations for Rad53, Cai et al. noted that the Chk2 interkinase interfaces display high temperature factors and disordered regions [29]. It is possible that subtle differences in the dimer arrangement between the Rad53 and Chk2 structure are a result of the presence of the FHA domain and FHA–kinase linker in Chk2, which forms extensive intramolecular interactions with the kinase N-lobe. It is also possible that kinase dimerization is inherently flexible or transient in nature, such that our Rad53 crystal structure captured an alternative mode of dimerization within the activation process. Consistent with this idea, the structure of the isolated human Chk2 kinase domain displays a very different head-to-head, tail-to-tail mode of dimerization (Fig. 4E) [30]. Despite employing altogether different modes of face-to-face dimerization, both modes support the potential for exchange of common secondary structure elements.

3.5. Disruption of Rad53 dimerization decreases Rad53 kinase activity in vitro

We speculated that the face-to-face dimerization mode observed in our Rad53 crystal structure might facilitate trans-autophosphorylation of Thr354 on the activation loop and thus impact Rad53 activation, as proposed for human Chk2 [30,32,35]. To test this model, we mutated conserved residues of the dimer interface and assessed catalytic function using an *in vitro* kinase assay (Fig. 5). Since we wished to assess trans-autophosphorylation as a measure of kinase activity, each Rad53 protein fragment (donor kinase) was tested for its ability to phosphorylate purified full-length kinase dead Rad53 protein (acceptor kinase; $Rad53^{FL:Dead}$, residues 1–821, 92 kDa) at Thr354. Phosphorylation was assessed by immunoblot using a Thr354 phospho-specific antibody (α-$Rad53^{pT354}$). Residues of the charge-mediated dimer interface were singly (D/A: D323A), doubly (DD/AA: D280/283A), or triply (DDD/AAA: D280/283/323A; KRK/AAA: K231A/R232A/K233A; KRK/EDE: K231E/R232D/K233E) mutated in the $Rad53^{170–512:Active}$ background to disrupt charge complementarity in the donor kinase. Residues of the conserved STQ-motif were also mutated to alanine (ATQ: S411A; SAQ: T412A; AAQ: S411A/T412A) in the $Rad53^{170–512:Active}$ background.

Single mutation of Ser411 (ATQ) or Asp323 (D/A) had little effect on the ability of the donor kinase to trans-autophosphorylate acceptor kinase $Rad53^{FL:Dead}$ at Thr354 (bottom panels: Fig. 5A, compare lane 6 to 3, and Fig. 5B, compare lane 4 to 2). In contrast, mutation of Thr412 (SAQ), double mutation of the acidic patch (DD/AA) and triple mutation of the basic patch (KRK/AAA) drastically reduced levels of trans-autophosphorylation (bottom panels: Fig. 5A, compare lane 9 to 3, and Fig. 5B, compare lanes 6 and 10 to 2, respectively). However, the level of Thr354 autophosphorylation of these mutants and wild type $Rad53^{170–512:Active}$ was similar (top panels: Fig. 5A, compare lanes 7–9 to 1–3, and Fig. 5B, compare lanes 3–4, 5–6, 9–10 to 1–2), suggesting that autophosphorylation of this site is fully saturated in bacterially produced Rad53 protein. Notably, mutation of Ser411 and Thr412 in tandem (AAQ), triple mutation of the acidic patch (DDD/AAA), and charge-reversal mutation of the basic patch (KRK/EDE) significantly reduced both trans-autophosphorylation (bottom panels: Fig. 5A, compare lane 12 to 3, and Fig. 4B, compare lanes 8 and 12 to 2) and autophosphorylation on Thr354 (top panels: Fig. 5A, compare lanes 10–12 to 1–3, and Fig. 5B, compare lanes 7–8 and 11–12 to 1–2). These results indicate that the Rad53 dimer interface is important for autophosphorylation, and that disruption of the dimer interface decreases autophosphorylation in a manner proportional to the predicted extent of dimer disruption.

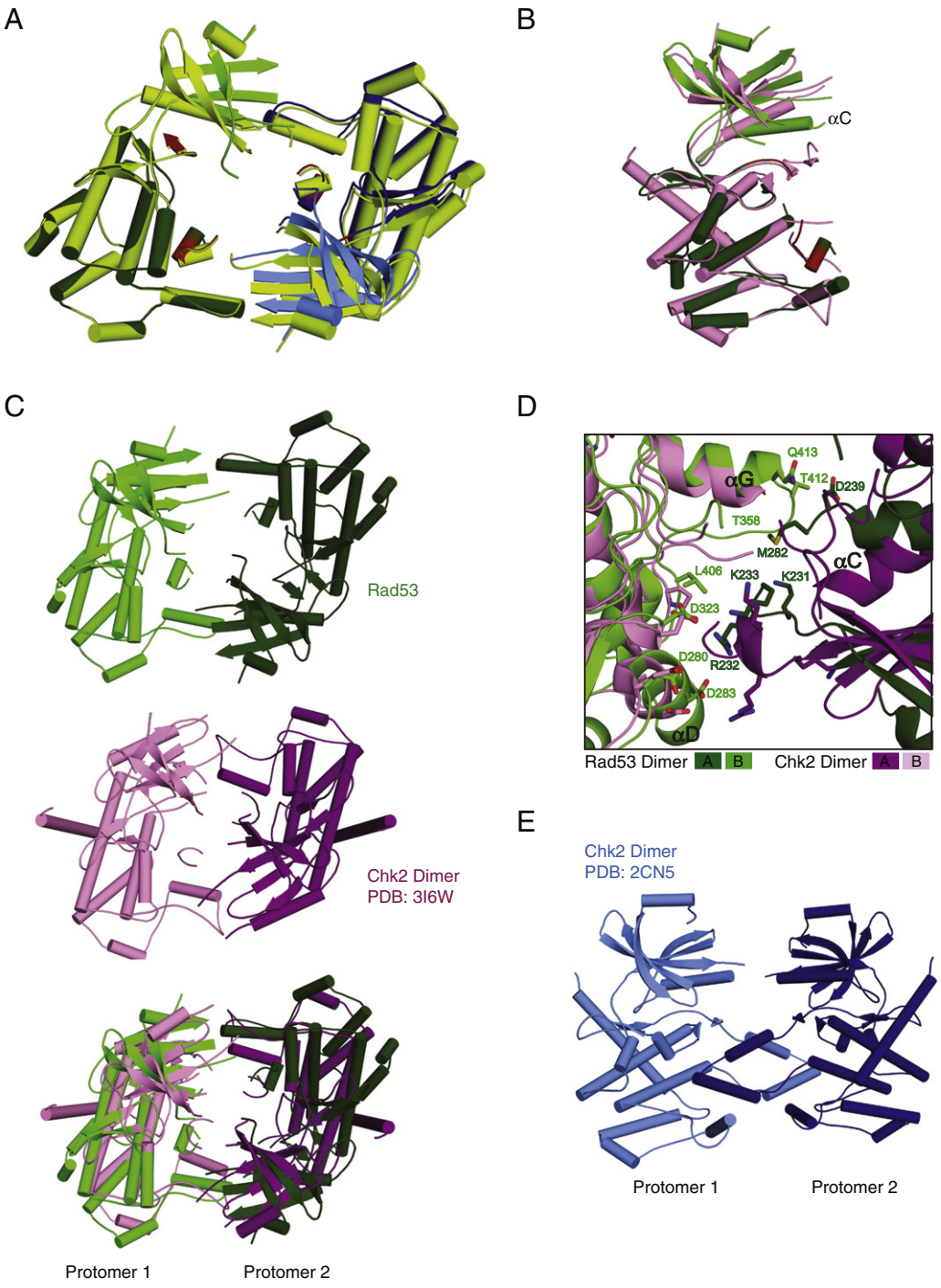

Fig. 4. Rad53 and Chk2 dimerize in a similar manner. Superpositions of the main chain atoms of Rad53 and Chk2 dimers. For clarity, SCD2 of Rad53 and the FHA domain of Chk2 are not shown. (A) Rad53 dimers 1 and 2, with dimer 1 colored lime green, and dimer 2 colored as in Fig. 3C. (B) Rad53 dimer 2 and Chk2 PDB 3I6W, with molecule B of Rad53 colored as in Fig. 3B and molecule B of Chk2 colored pink. (C) Rad53 dimer, Chk2 PDB 3I6W dimer, and superposition of the two dimers. (D) Magnification of the dimer interface, with molecules A and B of Rad53 colored dark and light green, respectively, and molecules A and B of Chk2 3I6U colored purple and pink, respectively. Residues proximal to the dimer interface are modeled and shown as stick, with carbon atoms colored according to their respective backbone and oxygen and nitrogen atoms colored red and blue, respectively. (E) Dimer of isolated Chk2 kinase domain, with molecules A and B colored light and dark blue (PDB: 2CN5).

To verify the importance of the dimer interface and investigate the possibility that the Rad53 mutations simply disrupted catalytic function, we generated dimer interface mutants in the kinase-dead acceptor background and assessed the ability of $Rad53^{FL:Active}$ donor kinase to trans-autophosphorylate Thr354. Mutation of the STQ-motif ($Rad53^{170–512:Dead(AAQ)}$) or the acidic patch ($Rad53^{170–512:Dead(DDD/AAA)}$) did not appreciably affect trans-autophosphorylation of Thr354 by $Rad53^{FL:Active}$ (bottom panel: Fig. 5C, compare lanes 6 and 9 to 3, respectively). However, combined mutation of both dimerization elements ($Rad53^{512–Dead(AAQ\ +\ DDD\ /\ AAA)}$) completely abolished autophosphorylation of Thr354 (bottom panel: Fig. 5C, lane 12). This is consistent with our findings that preservation of the face-to-face dimer interface is imperative to Thr354 autophosphorylation in trans.

To test the functional relevance of the dimer interface in full-length Rad53, we generated mutants in $Rad53^{FL:Active}$ donor kinase and

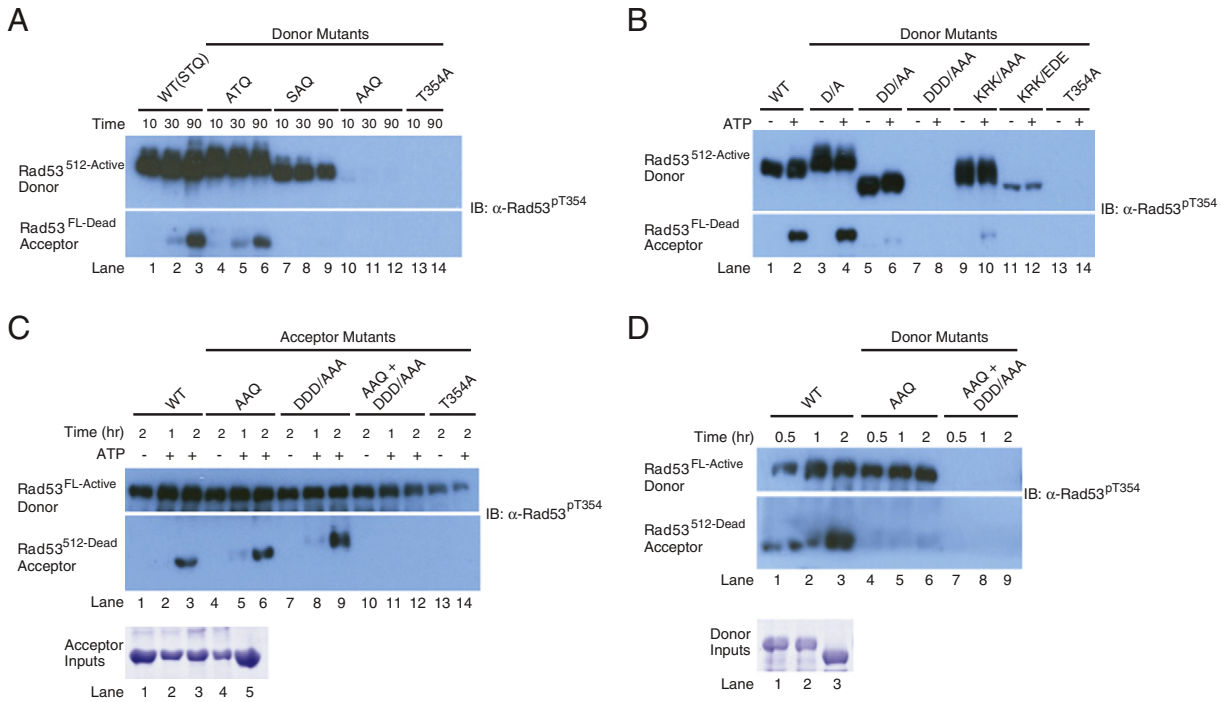

Fig. 5. Mutagenesis of the dimer interface decreases catalytic function. The ability of Rad53 donor proteins to autophosphorylate and to phosphorylate Rad53 acceptor proteins was assessed using an *in vitro* kinase assay. Westerns immunoblotted with α-Rad53^{pT354} are shown. (A) Donor Rad53$^{512-Active}$ proteins were assessed at time points of 10, 30, and 90 min. (B) Donor Rad53$^{512-Active}$ proteins were assessed in the presence (+) or absence (−) of ATP. (C) Donor Rad53$^{FL-Active}$ was assessed at 1 or 2 hour time points, in the presence (+) or absence (−) of ATP. An SDS-PAGE gel stained with Coomassie blue (bottom panel) shows acceptor inputs as follows: (1) WT, (2) AAQ, (3) DDD / AAA, (4) AAQ + DDD / AAA, and (5) T354A. (D) Donor Rad53$^{FL-Active}$ proteins were assessed at time points of 0.5, 1, or 2 h. An SDS-PAGE gel stained with Coomassie blue (bottom panel) shows donor inputs as follows: (1) WT, (2) AAQ, and (3) AAQ + DDD / AAA.

assessed their ability to phosphorylate Thr354 in catalytically dead Rad53 acceptor kinase (Rad53$^{170–512:Dead}$). Double STQ-motif mutant AAQ was autophosphorylated on Thr354 out of bacteria but showed a significant decrease in trans-autophosphorylation of acceptor kinase (bottom panel: Fig. 5D, compare lanes 4–6 to 1–3). Moreover, combined mutation of STQ and the charge-mediated interface (AAQ + DDD / AAA) resulted in the loss of both autophosphorylation and trans-autophosphorylation activities (Fig. 5D, compare lanes 7–9 to 1–3). These results suggest that the dimer interface as observed in our Rad53 crystal structure is required for Thr354 phosphorylation in full-length Rad53.

To verify the impact of mutating the dimer interface on the oligomerization status of Rad53, we performed analytical ultracentrifugation (AUC) analyses on Rad53 mutant proteins. At the relatively high protein concentrations utilized in AUC studies, mutants AAQ and DDD/AAA remained as dimers in solution, whereas mutant AAQ + DDD/AAA existed as a monomer (Fig. 6). Taken together, our mutagenic analyses indicate that the Rad53 dimer configuration revealed in our structure analyses is sampled in solution and is important for autophosphorylation *in vitro*.

3.6. Disruption of the Rad53 dimer reduces Rad53 activity in vivo

To ascertain whether mutation at the dimer interface leads to a loss of Rad53 activity *in vivo*, we generated yeast expression mutants in the full-length Rad53 wild-type background and tested them for cell viability following DNA damage. Loss-of-function of Rad53 results in DNA damage sensitivity, which is detected by monitoring yeast cell growth on media containing hydroxyurea (HU), a DNA damaging reagent. Mutation of the Rad53 dimer interface resulted in a significant loss of Rad53 function *in vivo* (Fig. 7). Single (D/A) or double (DD/AA) mutation of the charge-mediated dimer interface significantly impaired cell growth following DNA damage, while triple (DDD/AAA and KRK/EDE) mutation completely abolished cell growth on hydroxyurea. While mutation of the conserved STQ-motif to either AAQ or EEQ was well tolerated by the yeast cells, combined mutation of STQ and the charge-mediated interface (AAQ + DD / AA) resulted in stronger loss-of-function relative to DD/AA mutation alone. Together, our results indicate that the face-to-face mode of dimerization observed in the Rad53 crystal structure is functionally relevant for the ability of Rad53 to support the response to DNA replication stress in yeast.

3.7. Probing the potential for intermolecular strand exchange in the Rad53 dimer

An intriguing possibility raised by the Rad53 face-to-face dimer structure is the potential for intermolecular exchange of the activation segment and helix αEF to the active site of the adjacent Rad53 molecule. An intermolecular helix αEF strand-exchange phenomenon has been observed in a number of protein kinase face-to-face dimer structures, including originally human Chk2 [30], and subsequently DAPK3, SLK, LOK, and p38α MAPK, and has been proposed to represent an essential intermediate in the trans-autophosphorylation process [32,34,35]. Given that Rad53 is the yeast ortholog of human Chk2, we probed the potential for strand exchange in the Rad53 dimer.

Although helix αEF is well ordered in the Rad53 structure, we could not unequivocally determine whether this helix lies in an intramolecular position or if it is intermolecularly exchanged across the face-to-face dimer to the adjacent Rad53 molecule due to disorder of the loops connecting helix αEF to the kinase domain. An invariant salt bridge stabilizes the association of helix αEF with the kinase C-lobe [48]; Glu365 in helix αEF and Arg454 in loop αI–αJ mediate this interaction in Rad53 (Fig. 8A). We predicted that mutation of either residue to opposite polarity would perturb kinase function in part by destabilizing the association of helix αEF with the kinase domain (Fig. 8Bi and ii). Furthermore, if intermolecular association of helix αEF is critical for trans-autophosphorylation of Thr354 and Rad53 activation, then combining two charge reversal

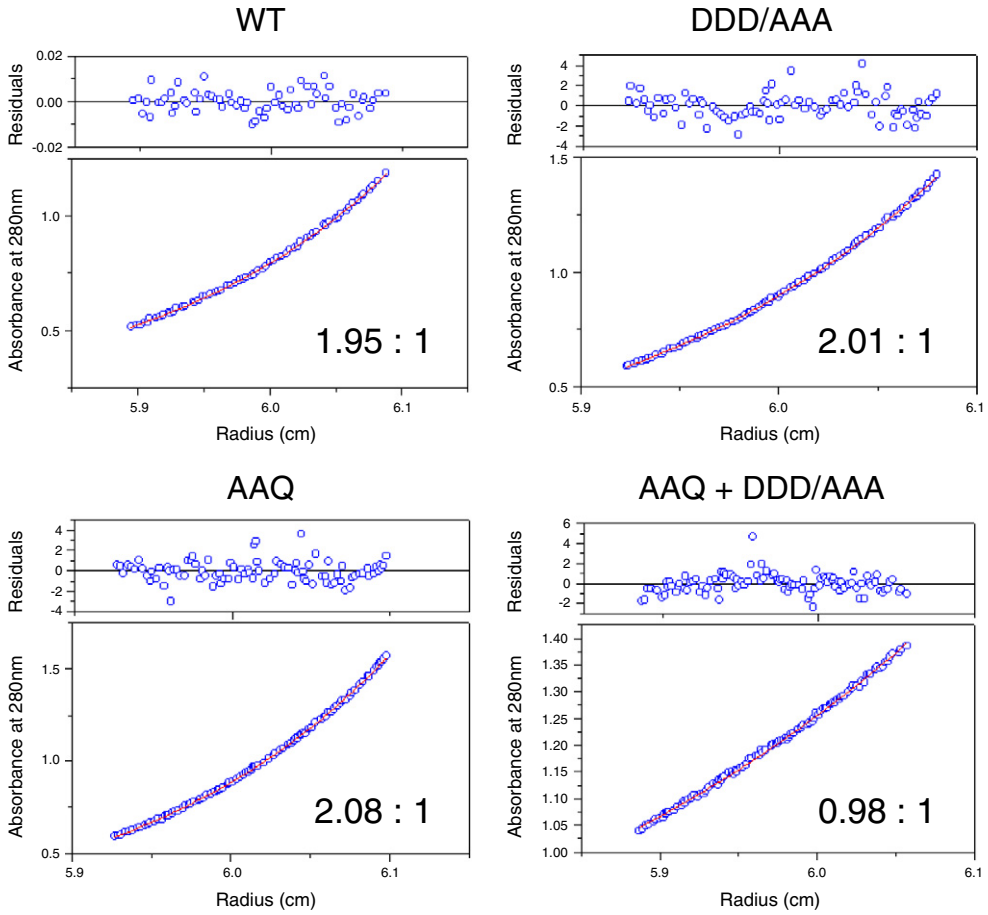

Fig. 6. Mutagenesis of the dimer interface disrupts dimerization. Data from analytical ultracentrifugation sedimentation equilibrium experiments are shown for Rad53 proteins. The data points depicted were collected at 10,000 rpm and 20 °C for WT, and 4 °C for Rad53 dimer mutants. The red lines in the lower panels correspond to the fit of the data to a monodisperse dimeric or monomeric model. The residual deviations from the theoretical fits are given in the upper panels.

mutants might restore catalytic function to the paired Rad53 proteins by reconstituting the stabilizing salt bridge interaction but with opposite polarity (Fig. 8Biii).

To test this possibility, two single site charge reversal mutations, Glu365Lys and Arg454Glu, were generated in the Rad53$^{170–512:Active}$ background on vectors with different antibiotic-resistance markers to

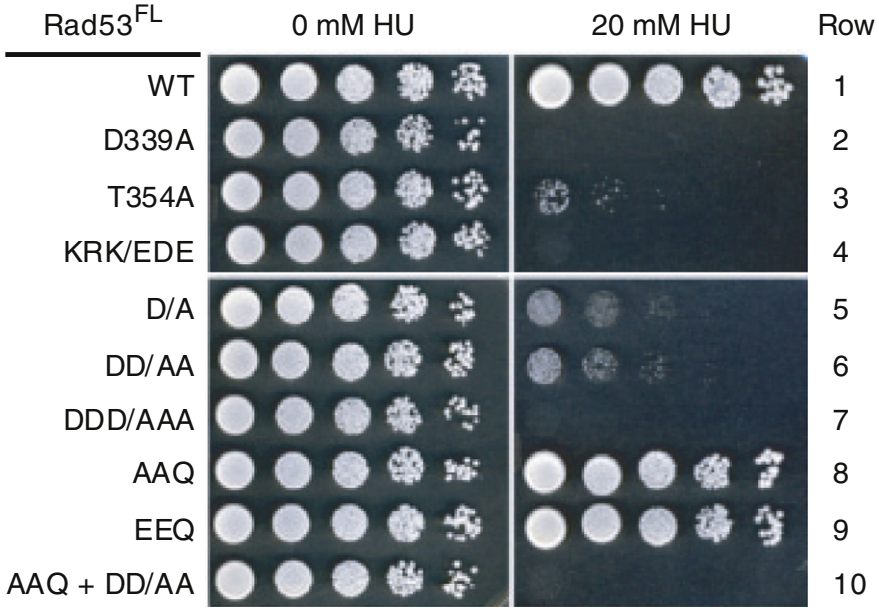

Fig. 7. Disruption of the Rad53 dimer reduces Rad53 activity *in vivo*. Strains containing Rad53 WT or mutant alleles were diluted serially five-fold and spotted on agar plates containing 0 mM or 20 mM hydroxyurea.

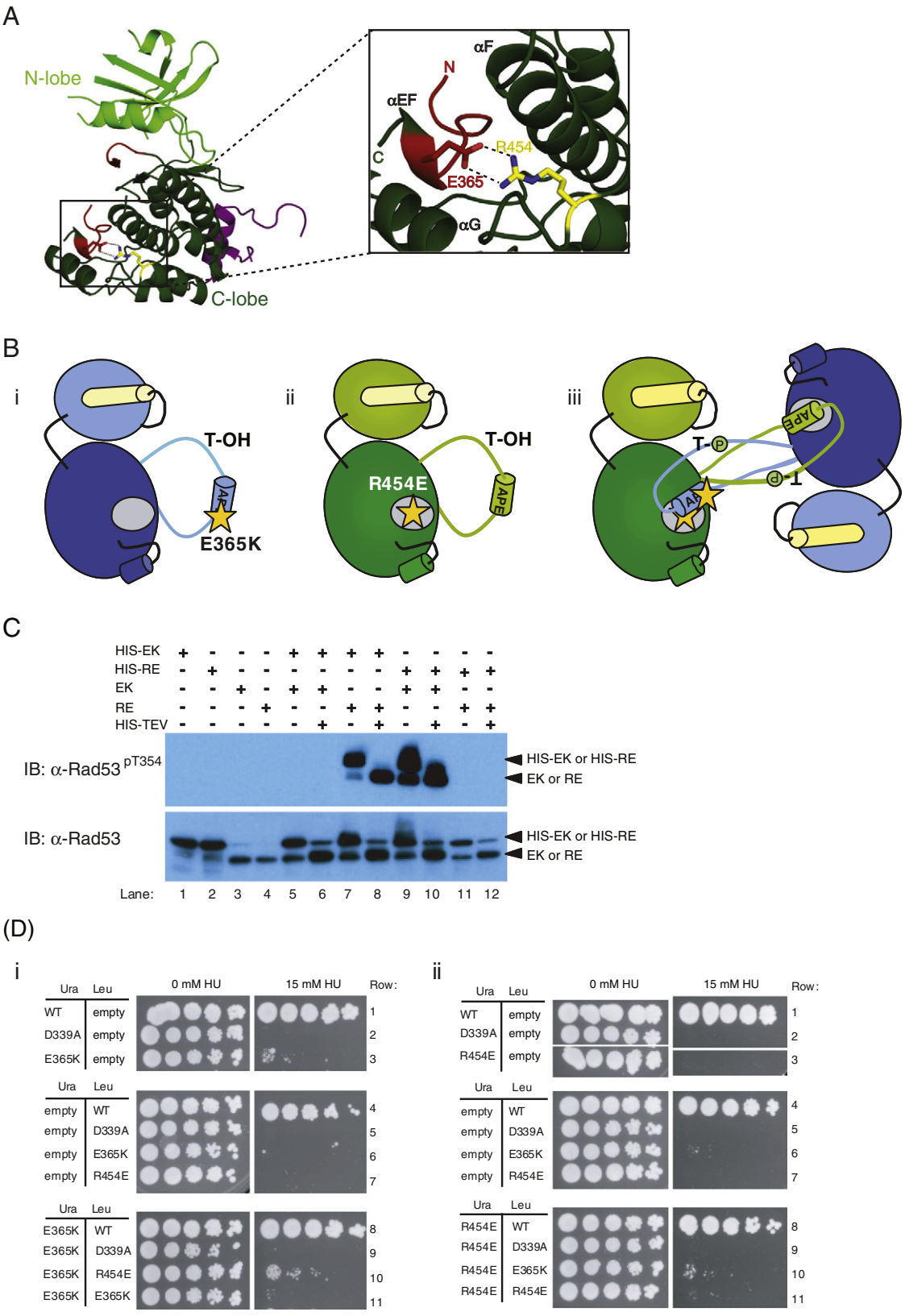

Fig. 8. Intermolecular strand exchange can occur in the Rad53 dimer. (A) Ribbon representation of the Cα atoms of the Rad53 kinase domain and SCD2, with the N-lobe, C-lobe, activation segment, and SCD2 colored as in Fig. 2. The boxed area is magnified, with Glu365 in helix αEF and Arg454 in loop αI–αJ shown as stick. Hatched lines represent the invariant salt bridge formed between Glu365 and Arg454. (B) Cartoon representation of Rad53 monomers with Thr354 indicated by T–OH and (i) Glu365Lys or (ii) Arg454Glu mutations indicated by a yellow star. In panel (iii), the Rad53 dimer is shown, with mutations indicated as in (i) and (ii) and phosphorylated Thr354 indicated by T–P. (C) Westerns immunoblotted with α-Rad53^{pT354} or α-Rad53. (D) Strains containing Rad53 WT or mutant alleles were singly expressed or coexpressed under selecting conditions, diluted serially five-fold and spotted on agar plates containing 0 mM or 15 mM hydroxyurea.

enable both single expression and coexpression in bacteria. The ability of mutant proteins to phosphorylate on Thr354 was assessed by α-Rad53^{pT354} immunoblot of whole cell bacterial lysates (Fig. 8C). Both single site mutant proteins Glu365Lys and Arg454Glu were completely compromised for their ability to phosphorylate on Thr354 when expressed alone (Fig. 8C, lanes 1–4, 5–6 and 11–12). However, coexpression of mutants Glu365Lys and Arg454Glu restored the ability of both proteins to be phosphorylated on Thr354 (Fig. 8C, lanes 7 and 9). Removal of the His-tag from mutants Glu365Lys and Arg454Glu by the addition of a His-TEV protease did not affect their ability to be phosphorylated on Thr354 (Fig. 8C, lanes 8 and 10). These complementation results strongly support the ability for intermolecular strand exchange of the activation segment and helix αEF in Rad53.

To determine whether coexpression of the Rad53 mutant proteins would functionally complement *in vivo*, we tested their ability to rescue yeast growth following DNA damage. Mutations Glu365Lys and Arg454Glu were introduced in the Rad53 full-length wild-type background on vectors with different selection markers (Ura and Leu) for single expression and coexpression in yeast cells. Both single site mutants were severely compromised for rescue of yeast cell growth following DNA damage compared to WT Rad53 (Fig. 8D, panels i and ii, compare row 3 to 1, and 6–7 to 4). Notably, coexpression of mutants Glu365Lys and Arg454Glu restored yeast cell growth, as compared to the growth observed when single mutants were coexpressed by themselves or with the Rad53$^{FL:Dead(D339A)}$ negative control (Fig. 8D, panels i and ii, compare row 10 to 11 and 9). These complementation results demonstrate partial rescue of Rad53 activation *in vivo*. It is clear that the degree of rescue provided by coexpression of the two single site mutants is still far less than that provided by WT Rad53. We reason that this may reflect the fact that once activated by trans-autophosphorylation in the context of a face-to-face dimer, Rad53 transitions to a monomer to phosphorylate downstream targets [25,29,49]. Under monomeric conditions, the single site mutants would not function optimally.

4. Discussion

The serine/threonine protein kinase Rad53 from budding yeast and its mammalian ortholog Chk2 are key regulators of the DNA damage checkpoint. Thus, activation of Rad53 must be tightly regulated to ensure maintenance of genomic stability. Given that Chk2 is known to dimerize in an FHA-dependent manner and that dimerization is required for Chk2 activation [23–28], we sought to investigate the role of dimerization in activating Rad53.

We have shown that Rad53 kinase can dimerize in solution and in a crystal environment. While each monomer adopts the bilobal-fold typical of a serine/threonine kinase domain, the molecules dimerize in a head-to-tail, face-to-face manner. Disruption of the dimer interface by mutagenesis resulted in a significant decrease in Rad53 activation *in vitro*, and significant loss-of-function and DNA damage sensitivity in yeast cells, thus confirming the functional relevance of the Rad53 dimer and revealing that Rad53 activation is driven by dimerization.

In order to catalyze a phosphorylation event, protein kinases require the precise orientation of their catalytic residues as well as ATP and the protein substrate. The same requirement for precise orientation of these elements exists whether the protein substrate is a downstream signaling molecule or the activation loop regulatory site of an adjacent kinase molecule. The conformation of the N-terminal DFG anchor and the C-terminal APE anchor is maintained in all active protein kinases, serving to anchor the activation segment [47]. An invariant salt bridge between a Glu residue in helix αEF of the APE anchor and an Arg residue from loop αI–αJ stabilizes the association of helix αEF with the kinase C-lobe [48]. Thus, this salt bridge is imperative to the formation of the APE anchor. Notably, this crucial interaction is maintained in the Rad53 dimer structure (Glu365 and Arg454) and other dimeric kinase structures where intermolecular strand exchange has been observed, including OSR1 kinase, SLK, p38α MAPK, p70S6K1, and the structure of the isolated Chk2 kinase domain [30,31,33–35]. However, the functional importance of this interaction in promoting trans-autophosphorylation has not been previously shown.

Our results prove unequivocally that mutation of either Glu365 or Arg354 to a residue of opposite polarity abolishes Rad53 kinase activity, indicating the functional importance of these residues in stabilizing the APE anchor point and promoting kinase activation. Moreover, our results demonstrate that Rad53 activation is restored when mutants of opposite polarity are coexpressed in bacteria or yeast cells. This shows that intermolecular strand exchange of the activation segment and helix αEF can occur in Rad53 *in vivo*, and provides functional evidence that activation segment exchange promotes Rad53 trans-autophosphorylation and kinase activation.

Overall, the mode of dimerization observed in our crystal structure of Rad53 was similar to that observed in a crystal structure of Chk2 consisting of the FHA and kinase domains [29]. Notably, both structures exhibited the potential for intermolecular activation segment exchange across the face-to-face dimer. Activation segment exchange was explicitly observed in the crystal structure of the isolated Chk2 kinase domain [30]. In that crystal structure, the kinase domains adopt an alternative tail-to-tail, face-to-face mode of dimerization in which the kinase domains do not interact except for activation segment exchange between protomers. Taken together, these structures suggest that there is a degree of conformational plasticity in Rad53/Chk2 dimerization and that activation segment exchange may contribute significantly to kinase dimerization and activation in Rad53/Chk2. Consistent with this inference, the interkinase interfaces in both the Rad53 and Chk2 FHA/kinase domain structures exhibit high temperature factors, disordered regions, and positional variation, which suggests that their contribution to dimerization is transient [29]. This may explain why single mutation of the dimer interfaces in Rad53 was often tolerated in our functional assays, while more extensive mutation of entire motifs or combination of motifs significantly decreased Rad53 activation.

The phenomenon of intermolecular strand exchange provides an additional layer of complexity in the regulation of protein kinases. Sequence alignment neither predicts which kinases exchange activation segments, nor explains why these proteins exchange segments [31]. Furthermore, the functional implication of strand exchange is not always apparent given that intermolecular strand exchange has been observed for OSR1 kinase and p70 ribosomal S6 kinase even though these kinases do not seem to undergo autophosphorylation [31,33]. Further experimental evidence is required to understand what elicits strand exchange and to validate the generality of this mechanism of kinase activation [32].

5. Conclusions

Rad53 can form dimers in solution and the kinase domain is sufficient for dimerization (Fig. 1). The crystal structure of Rad53 revealed that the kinase domains dimerize in a head-to-tail, face-to-face manner *via* conserved elements of the kinase N-lobe and C-lobe (Fig. 3). The mode of dimerization for Rad53 kinase is consistent with that of human Chk2, although the dimer interface appears to be transient and dynamic in nature (Fig. 4). Disruption of the Rad53 dimer interface by mutation of conserved residues results in the loss of dimerization (Fig. 6), reduces the ability of Rad53 to trans-autophosphorylate Thr354 *in vitro* (Fig. 5), and causes sensitivity to DNA damage in yeast cells (Fig. 7). These results indicate the functional relevance of the Rad53 dimer as observed in our crystal structure, and reveal the importance of this mode of head-to-tail, face-to-face dimerization for Rad53 activation. Disruption of the invariant salt bridge between Glu365 of helix αEF and Arg354 of loop αI–αJ abolishes Rad53 kinase activity *in vitro* and results in sensitivity to DNA damage, indicating the importance of these residues in stabilizing the APE anchor point of the activation segment (Fig. 8). Rad53 activation is restored when mutants of opposite polarity are coexpressed in bacteria or yeast cells, showing

that intermolecular strand exchange can occur in Rad53 and may promote Rad53 kinase activation.

Accession numbers

Coordinates and structure factors have been deposited in the Protein Data Bank with accession numbers 4PDP and 4PDS.

Contributors

LEW-G refined the structures, analyzed the data, and prepared the manuscript; CSH crystallized, solved, and refined the structures and performed biochemical experiments; FDS performed yeast functional assays; DFC refined the structures; CJM supervised LEW-G; DD and FS supervised the project and wrote the manuscript. All authors approve the final article.

Acknowledgments

This work was supported by grants from the Canadian Institutes of Health Research to F.S. (MOP36399), D.D. (MOP89754), and C.J.M. (MOP12859). F.S. and D.D. are supported by the Canada Research Chairs (Tier 1). D.D. is also supported by a Thomas Kierans Chair in Molecular Mechanisms of Cancer.

References

[1] S.P. Jackson, J. Bartek, Nature 461 (2009) 1071–1078.
[2] D. Durocher, S.P. Jackson, Curr. Opin. Cell Biol. 13 (2001) 225–231.
[3] J. Rouse, S.P. Jackson, Science 297 (2002) 547–551.
[4] J. Bartek, J. Lukas, Cancer Cell 3 (2003) 421–429.
[5] C.W. Moore, Mutat. Res. 51 (1978) 165–180.
[6] J.B. Allen, Z. Zhou, W. Siede, E.C. Friedberg, S.J. Elledge, Genes Dev. 8 (1994) 2401–2415.
[7] T.A. Weinert, G.L. Kiser, L.H. Hartwell, Genes Dev. 8 (1994) 652–665.
[8] A.G. Paulovich, L.H. Hartwell, Cell 82 (1995) 841–847.
[9] D.S. Fay, Z. Sun, D.F. Stern, Curr. Genet. 31 (1997) 97–105.
[10] S. Matsuoka, M. Huang, S.J. Elledge, Science 282 (1998) 1893–1897.
[11] A. Blasina, I.V. de Weyer, M.C. Laus, W.H. Luyten, A.E. Parker, C.H. McGowan, Curr. Biol. 9 (1999) 1–10.
[12] A. Hirao, Y.Y. Kong, S. Matsuoka, A. Wakeham, J. Ruland, H. Yoshida, D. Liu, S.J. Elledge, T.W. Mak, Science 287 (2000) 1824–1827.
[13] Z. Sun, D.S. Fay, F. Marini, M. Foiani, D.F. Stern, Genes Dev. 10 (1996) 395–406.
[14] D.F. Stern, P. Zheng, D.R. Beidler, C. Zerillo, Mol. Cell. Biol. 11 (1991) 987–1001.
[15] D. Durocher, J. Henckel, A.R. Fersht, S.P. Jackson, Mol. Cell 4 (1999) 387–394.
[16] A. Traven, J. Heierhorst, Bioessays 27 (2005) 397–407.
[17] K. Finn, N.F. Lowndes, M. Grenon, Cell Mol. Life Sci. 69 (2012) 1447–1473.
[18] Z. Sun, J. Hsiao, D.S. Fay, D.F. Stern, Science 281 (1998) 272–274.
[19] J.E. Vialard, C.S. Gilbert, C.M. Green, N.F. Lowndes, EMBO J. 17 (1998) 5679–5688.
[20] A. Emili, Mol. Cell 2 (1998) 183–189.
[21] M.F. Schwartz, J.K. Duong, Z. Sun, J.S. Morrow, D. Pradhan, D.F. Stern, Mol. Cell 9 (2002) 1055–1065.
[22] E.S. Chen, N.C. Hoch, S.C. Wang, A. Pellicioli, J. Heierhorst, M.D. Tsai, Mol. Cell. Proteomics 13 (2014) 551–565.
[23] C.H. Lee, J.H. Chung, J. Biol. Chem. 276 (2001) 30537–30541.
[24] J.K. Schwarz, C.M. Lovly, H. Piwnica-Worms, Mol. Cancer Res. 1 (2003) 598–609.
[25] J.Y. Ahn, X. Li, H.L. Davis, C.E. Canman, J. Biol. Chem. 277 (2002) 19389–19395.
[26] X. Xu, L.M. Tsvetkov, D.F. Stern, Mol. Cell. Biol. 22 (2002) 4419–4432.
[27] R. Melchionna, X.B. Chen, A. Blasina, C.H. McGowan, Nat. Cell Biol. 2 (2000) 762–765.
[28] S. Matsuoka, G. Rotman, A. Ogawa, Y. Shiloh, K. Tamai, S.J. Elledge, Proc. Natl. Acad. Sci. U. S. A. 97 (2000) 10389–10394.
[29] Z. Cai, N.H. Chehab, N.P. Pavletich, Mol. Cell 35 (2009) 818–829.
[30] A.W. Oliver, A. Paul, K.J. Boxall, S.E. Barrie, G.W. Aherne, M.D. Garrett, S. Mittnacht, L.H. Pearl, EMBO J. 25 (2006) 3179–3190.
[31] S.J. Lee, M.H. Cobb, E.J. Goldsmith, Protein Sci. 18 (2009) 304–313.
[32] A.W. Oliver, S. Knapp, L.H. Pearl, Trends Biochem. Sci. 32 (2007) 351–356.
[33] T. Sunami, N. Byrne, R.E. Diehl, K. Funabashi, D.L. Hall, M. Ikuta, S.B. Patel, J.M. Shipman, R.F. Smith, I. Takahashi, J. Zugay-Murphy, Y. Iwasawa, K.J. Lumb, S.K. Munshi, S. Sharma, J. Biol. Chem. 285 (2010) 4587–4594.
[34] U. Rothweiler, E. Aberg, K.A. Johnson, T.E. Hansen, J.B. Jorgensen, R.A. Engh, J. Mol. Biol. 411 (2011) 474–485.
[35] A.C. Pike, P. Rellos, F.H. Niesen, A. Turnbull, A.W. Oliver, S.A. Parker, B.E. Turk, L.H. Pearl, S. Knapp, EMBO J. 27 (2008) 704–714.
[36] F.D. Sweeney, F. Yang, A. Chi, J. Shabanowitz, D.F. Hunt, D. Durocher, Curr. Biol. 15 (2005) 1364–1375.
[37] C. Lusty, J. Appl. Crystallogr. 32 (1999) 106–112.
[38] Z. Otwinowski, W. Minor, in: C.W. Carter J., R.M. Sweet (Eds.), Methods in Enzymology, Academic Press, New York, 1997, pp. 307–326.
[39] W. Kabsch, Acta Crystallogr. D Biol. Crystallogr. 66 (2010) 125–132.
[40] P.D. Adams, P.V. Afonine, G. Bunkoczi, V.B. Chen, I.W. Davis, N. Echols, J.J. Headd, L.W. Hung, G.J. Kapral, R.W. Grosse-Kunstleve, A.J. McCoy, N.W. Moriarty, R. Oeffner, R.J. Read, D.C. Richardson, J.S. Richardson, T.C. Terwilliger, P.H. Zwart, Acta Crystallogr. D Biol. Crystallogr. 66 (2010) 213–221.
[41] A.T. Brunger, P.D. Adams, G.M. Clore, W.L. DeLano, P. Gros, R.W. Grosse-Kunstleve, J.S. Jiang, J. Kuszewski, M. Nilges, N.S. Pannu, R.J. Read, L.M. Rice, T. Simonson, G.L. Warren, Acta Crystallogr. D Biol. Crystallogr. 54 (1998) 905–921.
[42] P. Emsley, K. Cowtan, Acta Crystallogr. D Biol. Crystallogr. 60 (2004) 2126–2132.
[43] T.A. Jones, J.Y. Zou, S.W. Cowan, M. Kjeldgaard, Acta Crystallogr. A 47 (Pt 2) (1991) 110–119.
[44] G.N. Murshudov, P. Skubak, A.A. Lebedev, N.S. Pannu, R.A. Steiner, R.A. Nicholls, M.D. Winn, F. Long, A.A. Vagin, Acta Crystallogr. D Biol. Crystallogr. 67 (2011) 355–367.
[45] P. Kanellis, R. Agyei, D. Durocher, Curr. Biol. 13 (2003) 1583–1595.
[46] M. Huse, J. Kuriyan, Cell 109 (2002) 275–282.
[47] B. Nolen, S. Taylor, G. Ghosh, Mol. Cell 15 (2004) 661–675.
[48] S.S. Taylor, E. Radzio-Andzelm, Structure 2 (1994) 345–355.
[49] J. Ahn, C. Prives, J. Biol. Chem. 277 (2002) 48418–48426.